Ultrasonics 137 (2024) 107201

Contents lists available at ScienceDirect

Ultrasonics

journal homepage: www.elsevier.com/locate/ultras

A cascaded Nitinol Langevin transducer for resonance stability at elevated temperatures

Yuchen Liu, Mahshid Hafezi, Andrew Feeney *

Centre for Medical and Industrial Ultrasonics, University of Glasgow, James Watt School of Engineering, Glasgow, G12 8QQ, United Kingdom

ARTICLE INFO

Keywords:
Resonance stability
Cascaded transducer
Nitinol
Non-linear dynamics
Self-heating experiment

ABSTRACT

Across power ultrasonics and sensing, piezoelectric ultrasonic transducers commonly experience degradation in mechanical, electrical, and dynamic performance due to the relatively high sensitivity of piezoelectric materials to changes in temperature. These changes, arising for example through high excitation voltages or environmental conditions, can lead to nonlinear dynamic behaviours which compromise device performance. To overcome this, the excitation signal to the piezoelectric material is often pulsed, mitigating the influence of temperature rises. However, there remain constraints on suitable candidate piezoelectric materials for power ultrasonic devices. As a novel approach to mitigating the influence of temperature on the properties of piezoelectric materials, the phase-transforming shape memory alloy Nitinol is incorporated into the piezoelectric stack of a Langevin power ultrasonic transducer, in a cascade formation. The underlying principle is that the nonlinear hardening response of Nitinol to rising temperature can be used to dynamically compensate for the nonlinear softening of the piezoelectric materials. Thus, the dynamic response of the transducer can be linearised at elevated excitation levels. In this study, two configurations of Langevin transducer are designed and characterised. One transducer incorporates a Nitinol middle mass, and in the second, titanium. A combination of electrical and thermomechanical characterisation is undertaken, where it is demonstrated that the nonlinear softening of the piezoelectric stack can be mitigated through control of the Nitinol microstructure. The vibration amplitudes of the Nitinol-middle cascaded transducer are higher and more stable when the Nitinol is austenite rather than a combination of martensite and austenite at room temperature. It has also been shown that the vibration amplitude and resonance frequency of Nitinol-middle cascaded transducer remain stable as temperature changes from 20 °C to 45 °C, dependent of the excitation voltage. Moreover, the self-heating experiment demonstrates the resonance stability of the Nitinol-middle cascaded transducer for continuous operation.

1. Introduction

The Langevin transducer has been a popular configuration of ultrasonic device in power ultrasonics for many years, with broad application across a wide range of fields including motors and actuation [1], surgery [2], welding [3], and drilling [4]. Their operational modal responses are commonly tuned to low ultrasonic frequencies, principally between 20 kHz and 100 kHz, thus enabling the necessary micrometre-scale vibration amplitudes to meet the demands of industrial and surgical applications.

The Langevin transducer typically comprises a stack of piezoelectric rings sandwiched between two metallic end-masses and compressed with a centrally aligned bolt. The stress applied to compress the entire stack, via the bolt, allows sufficiently high vibration amplitudes to be generated without mechanical failure of the piezoelectric rings. It is common for the piezoelectric rings to be a hard form of lead zirconate titanate (PZT), for power ultrasonic applications. The piezoelectric properties of PZT are temperature dependent, where parameters such as the charge and voltage constants, d and g, and compliance and permittivity, s and ϵ, respectively, are highly sensitive to temperature [5,6]. Hence, both the dynamic characteristics of the piezoelectric Langevin ultrasonic transducer, including resonance frequency and vibration amplitude, and electromechanical parameters including impedance, are highly temperature dependent [7–9]. There are emerging applications for Langevin transducers in environments of elevated temperature [10], notwithstanding contemporary approaches to mitigate the influence of temperature in the stack.

A commonly applied technique to mitigate the influence of temperature in the piezoelectric stack is through pulse-excitation [11], where

* Corresponding author.
E-mail address: Andrew.Feeney@glasgow.ac.uk (A. Feeney).
URL: https://www.gla.ac.uk/schools/engineering/staff/andrewfeeney/ (A. Feeney).

https://doi.org/10.1016/j.ultras.2023.107201
Received 10 October 2023; Accepted 9 November 2023
Available online 10 November 2023

the time window for which the piezoelectric material is subjected to voltages causing temperature increases is minimised, and the measurement of the dynamic performance of the transducer is undertaken at steady-state. However, the principal disadvantage of this technique is that relatively long burst times can still be required to ensure steady state, and there remain temperature increases in the piezoelectric materials. An alternative approach is to compensate for temperature rises, and thus nonlinear behaviour, by phase tracking. Here, the changing resonance response of the transducer as a function of the excitation is monitored and the excitation adjusted accordingly. However, the dynamic properties of the transducer, including resonance frequency, are still a function of temperature. A further practical option is to apply a DC bias voltage across the transducer to compensate for the frequency shift in part generated by changes in temperature [12]. However, DC bias voltages can result in unstable load powers and vibration amplitudes with respect to temperature. In general, mitigating the influence of temperature on the performance of piezoelectric ultrasonic transducers remains a significant challenge for practical applications.

In recent years, there has been an emerging focus on integrating shape memory materials, principally nickel titanium, or Nitinol, into ultrasonic transducers [13–15]. The underlying motivation of these studies was to investigate mechanisms by which transducers with adaptive dynamics could be engineered by using materials with phase-transformational properties. Specifically, the elastic moduli of Nitinol are highly dependent on even modest changes in temperature, and it was demonstrated that the resonance frequencies and associated modes could be shifted in the order of kHz, in transducers fabricated from Nitinol.

In general, Nitinol is a binary alloy of nickel and titanium, and it is used in aerospace, medical, and industrial applications [16,17], principally for damping and micro-actuator systems. Nitinol possesses two key mechanical properties which are dependent, in part, on temperature. One is the shape memory effect, the ability of the material to recover a particular set shape in response to temperature, and the other is superelasticity, which is the ability of the material to recover from relatively high levels of applied stress [18]. Both phenomena arise from the phase transition between martensite and austenite microstructures, where martensite typically manifests at lower temperatures, relatively, and austenite appears at higher temperatures. An intermediate orthorhombic phase, known as the R-phase, can also be generated, depending on the composition of the alloy. These microstructures all possess different elastic properties, varying from a modulus in the order of 30–40 GPa for martensite [19,20], towards 70–90 GPa for austenite [21,22]. Fundamentally, the temperatures at which these microstructures can be generated depend on the alloy composition and the hot and cold working conditions to which the material is subjected. Variations in modulus have been studied using techniques such as nanoindentation [23], resonant ultrasound spectroscopy (RUS) [24], and tensile testing [19]. Measurement of the modulus change in a specimen of Nitinol thus enables the design of ultrasonic transducers with adaptive dynamic characteristics, given the dependence of frequency on elastic modulus.

Up to this point, the integration of Nitinol into ultrasonic transducers has generally been limited to flextensional type configurations, such as the cymbal transducer [13], where the resonance frequencies for different modes of vibration were shown to be tuneable over thousands of Hz. Given the popularity of the Langevin transducer, and the continuing challenges associated with operational stability with regards to temperature, Nitinol presents a promising and practical opportunity to compensate for the influence of temperature on the dynamic performance of the transducer. In this research, a form of cascade transducer incorporating Nitinol is proposed, called a Nitinol-middle cascaded transducer (NMCT). Cascade transducers are a variant of the Langevin, typically incorporating a middle mass between two piezoelectric ceramic stacks to enable multi-frequency behaviours [25]. Here, Nitinol is embedded as the middle mass in a piezoelectric Langevin transducer, whose primary function is to compensate for thermally induced nonlinear behaviours of the PZT stack.

In this study, two transducers are designed and fabricated. The first is the NMCT, and the second incorporates a titanium middle mass in place of the Nitinol, called the titanium-middle cascaded transducer (TMCT). The purpose of fabricating the TMCT is to demonstrate the unique behaviours regarding compensation of the dynamics for the NMCT, as a comparison case. First, the phase transition temperatures of the Nitinol were measured through differential scanning calorimetry (DSC). Electrical discharge machining (EDM) was used to fabricate the Nitinol ring for the NMCT, and both transducers were then assembled. The electrical properties of each were measured using electrical impedance analysis (EIA), and the dynamic characteristics were obtained through laser Doppler vibrometry (LDV). Using these techniques, it can be demonstrated that through the control of the moduli of a Nitinol ring embedded in a Langevin transducer, the thermally induced softening of the PZT stack (a nonlinear reduction in resonance frequency), and its influence on the dynamic characteristics of the transducer, can be compensated. The wider aim of this research is to enable the development of Langevin transducers for operation in hostile environments, for example cryogenics or high temperature welding.

2. Methodology

The transducers were designed using finite element analysis (FEA), where the resonance frequencies of the first longitudinal modes of vibration were tuned to around 30 kHz. Following this, the transducer components, including piezoelectric ceramic rings, were acquired, before the end and middle masses of the configurations were machined. A conventional machining process can be utilised for titanium, but Nitinol experiences relatively severe work hardening, and so here EDM was applied instead, to machine the Nitinol ring to the required dimensions [26]. Prior to these steps, the transformation properties of the Nitinol used to fabricate the NMCT were characterised.

2.1. Characterisation of Nitinol

A Nitinol cylinder (Kellogg's Research Labs), with a diameter of 25 mm was procured, with a 1.5 mm^3 sample prepared for DSC measurements. Prior to fabrication, the transformation temperatures of the Nitinol used for the NMCT were measured using DSC (DSC2A-01781, TA Instruments) with 50mL/min heat flow. The purpose of DSC here is to measure the key temperatures at which the transitions between different phase microstructures occur in the material, thus providing a guide for practical operation of the NMCT. Principally, the onset and completion of the formation of each phase microstructure can be measured, via individual temperature markers. These temperatures comprise the martensite start (M_s), martensite peak (M_p), martensite finish (M_f), austenite start (A_s), austenite peak (A_p), austenite finish (A_f), R-phase start (R_s), R-phase peak (R_p), and R-phase finish (R_f).

Heating and cooling rates were set to 10 °C/min, with a defined temperature range from −70 °C to 100 °C, to ensure all A_f to M_f temperatures would be captured. The nominal A_f of the material as supplied was 34.21 °C. The transformation temperatures of the Nitinol are shown in Fig. 1 from DSC.

In general, the phase transitions correspond to spikes in the heat flow. A single transition stage 'martensite → austenite' appears as the Nitinol sample is heated heating, whereas two transition stages 'austenite → R-phase' and 'R-phase → martensite' appear while cooling. It is common for an intermediate phase such as the R-phase to manifest on the cooling step, based on the fact that Nitinol is hysteretic in nature, and is important to consider for the dynamics of the NMCT whether the applied temperature is heating or cooling.

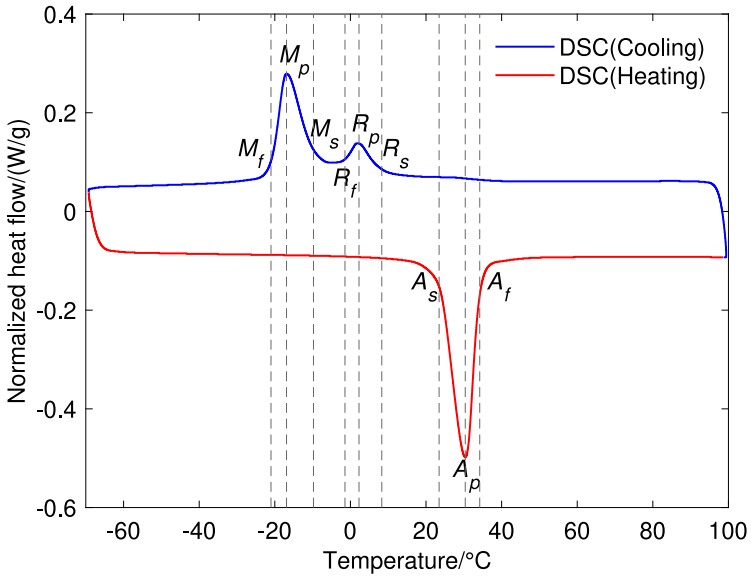

Fig. 1. DSC thermogram for the Nitinol used for the NMCT, where the measured transformation temperatures are indicated.

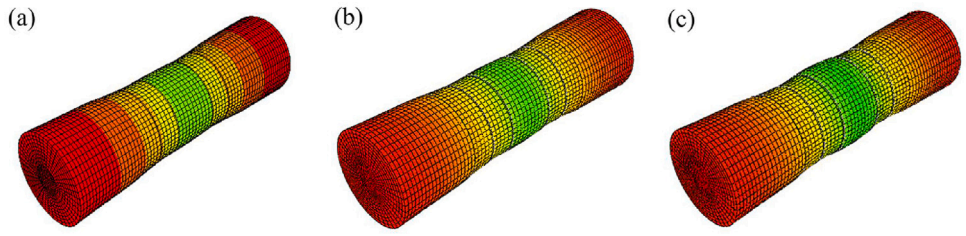

Fig. 2. Finite element simulation results of the first longitudinal mode for (a) the NMCT in the heating cycle at 28.705 kHz, (b) in the cooling cycle at 29.515 kHz and (c) the TMCT at 31.214 kHz.

2.2. Design of the transducers

A cascade configuration of Langevin transducer was produced using FEA software (Abaqus, Dassault Systèmes), with one model incorporating Nitinol as the middle mass to form the NMCT, and the other comprising a titanium ring as the middle mass, constituting the TMCT. The first longitudinal mode of each transducer was tuned to approximately 30 kHz, consistent with typical operational frequencies for common power ultrasonic applications, from 20 kHz to 100 kHz. The finite element results are shown in Fig. 2, along with the resonance frequencies.

The complexities surrounding estimating the elastic moduli of Nitinol are well documented [27,28]. For example, elastic moduli of the twinned martensite phase is highly dependent on detwinning and reorientation [29], and it should be noted that a key determining factor of modulus difference between martensite and austenite is the grain size [30]. The larger the grain size, the larger the modulus difference within the temperature range of −100 °C to 100 °C [31]. Therefore, at the outset, the finite element model for the NMCT was developed through an iterative trial approach using estimations of elastic modulus using the scientific literature [19–22], from where the models were later refined using experimental data. The material properties used in the final FEA models are shown in Table 1, which includes the iteratively defined elastic moduli for the Nitinol in its martensitic and austenitic phases.

The detailed configuration of the transducers is shown in Fig. 3, where the two end masses, the middle mass, and the two PZT stacks are indicated, alongside key dimensional labels which can be used for reference.

Table 1
Iteratively defined elastic moduli for the Nitinol in FEA.

Phase	Elastic moduli (GPa)
Mixed martensite and austenite (Room temperature in heating cycle)	60
Austenite (Room temperature in cooling cycle)	73

The Nitinol middle mass is a ring manufactured by EDM, with copper used as the electrode material because of its high thermal and electrical conductivity [32]. Each PZT stack (PZ26, CTS Corporation) consists of one pair of piezoelectric ceramic rings, and complemented by two copper electrodes. To ensure structural symmetry and uniformity, a bolt feature was fabricated on the front mass 2 to fit into each transducer assembly, where a threaded feature machined into the front mass 1.

A major challenge in the design of these transducers was accommodating differences in acoustic impedance between the end mass materials and the middle mass in each case. Acoustic impedance can be described as the product of material density and sound velocity, and it is known that an optimal acoustic performance is achieved when the sandwich structure possess a gradient acoustic impedance [33]. Measurements of longitudinal sound velocity through Nitinol were made using a pulse-echo system (DPR300 Pulse/Receiver, JSR Ultrasonics), where the data was collected by an oscilloscope (InfiniiVision DSOX2014A, Keysight Technologies). This enabled acoustic impedances for both mixed martensite and austenite (Heating cycle) and austenite (Cooling cycle) to be measured, where they are shown to be marginally higher than that of PZ26, as shown in Table 2.

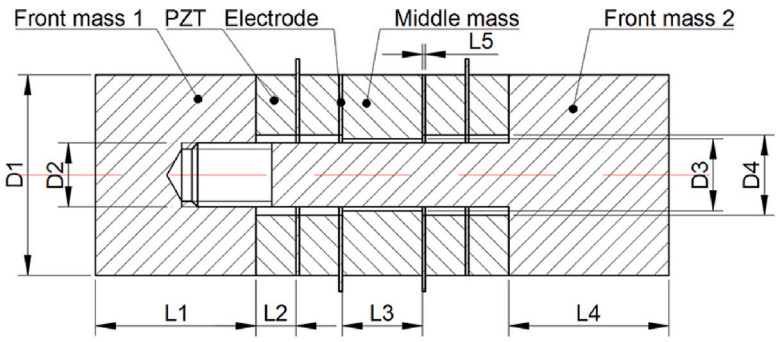

Fig. 3. Detailed schematic of the configuration used for both the NMCT and the TMCT.

Table 2
Acoustic impedances of transducer materials.

Material	Acoustic impedance ($kgm^{-2}s^{-1}$)
Nitinol (Heating)	33.1e6
Nitinol (Cooling)	34.9e6
PZ26	32.3e6 [34]
Aluminium (6082)	16.57e6 [35]
Titanium (Ti6Al4V)	25.694e6 [36]

Table 3
Configuration parameters.

Parameter	Dimension value (mm)
$L1$	20
$L2$	5
$L3$	10
$L4$	20
$L5$	0.38
$D1$	25
$D2$	8
$D3$	9
$D4$	10

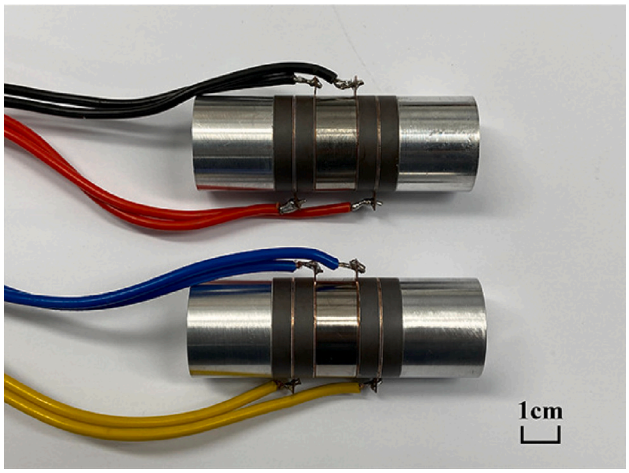

Fig. 4. Manufactured NMCT (top) and TMCT (bottom).

The measurements of acoustic impedance compare well with observations in the literature [37], although material properties of Nitinol alloys can differ, depending on their specific compositions and processing conditions. Using these measurements, a material with acoustic impedance lower than PZ26 would be desirable for front mass 1, with reference to Fig. 3, to ensure the necessary acoustic impedance gradient. An aluminium alloy (6082) was also selected, since its acoustic impedance is lower than that of both Nitinol and PZT, and because it has relatively low loss characteristics with high energy transmission [38]. Finally, titanium (Ti6Al4V) was selected for the TMCT since its acoustic impedance is close to that of Nitinol, and is a material commonly used in power ultrasonic transducers such as the Langevin configuration, like aluminium, in part because of its relatively high magnitude of quality factor. A summary of the dimensions for both transducers is shown in Table 3, with reference to Fig. 3.

The NMCT and TMCT were both assembled by loading the central bolt with a pre-stress of 10.5 Nm. It appears that a pre-stress of 10.5 Nm is optimal for achieving the lowest electric impedance for both transducers. The manufactured transducers are shown in Fig. 4.

2.3. Dynamic characterisation

Accurate mode identification is important during the experimental process because it should be ensured that the correct mode of vibration is being monitored as the associated resonance frequency changes with temperature. When the temperature of the transducer changes, the dynamic properties, particularly elastic modulus, of the transducers also change, thereby directly influencing resonance frequency. EIA generally only provides electrical data with respect to parameters including frequency, thus LDV is required to capture the modal behaviour which can be correlated with FEA. Here, the vibration modes of each transducer were measured at the room temperature using a 3D scanning laser Doppler vibrometer (MSA100, Polytec) under an 8 V_{P-P} excitation. The reason of measuring under 8 V_{P-P} is to ensure a sufficiently clear and detectable vibration mode shape. The LDV results for two transducers at room temperature for the first longitudinal mode of vibration are shown in Fig. 5.

During the heating cycle, the Nitinol undergoes a transformation from its low temperature martensite state to the high temperature austenite state. Conversely, during the cooling cycle, the Nitinol transitions from its high temperature austenite state to the low temperature martensite state. There is a hysteretic response inherent in shape memory materials such as Nitinol, as shown in Fig. 1, and this explains the resonance frequency difference of the NMCT across the heating and cooling cycles. These mode shapes can be directly compared with those shown in Fig. 2, where the measured resonance frequencies also closely match. Therefore, there is a high level of confidence in the estimations for the elastic moduli used for the NMCT model, provided in Section 2.2.

With the longitudinal mode for each transducer measured, along with its resonance frequency, the dynamic response of each transducer could then be monitored as a function of temperature. The aim of this part of the study was to quantify the influence of changing temperature on the dynamic properties of a transducer incorporating Nitinol (NMCT), with those for a transducer comprising a conventional Langevin transducer material, titanium (TMCT). To achieve this, resonance frequency and electrical impedance were monitored by an analogue circuit with an impedance analyser module (Analog Discovery 2, Digilent) which was connected to a commercial climate chamber

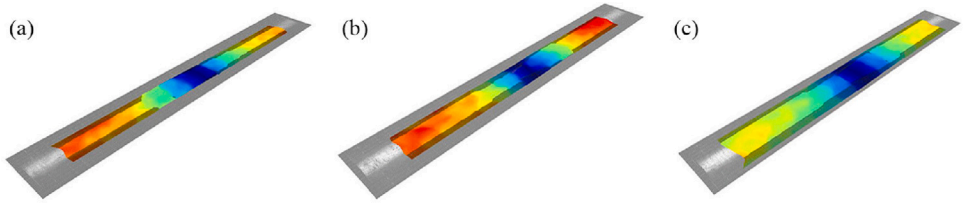

Fig. 5. LDV results of the first longitudinal mode for NMCT in the heating cycle (a) at 28.719 kHz and cooling cycle (b) at 29.336 kHz, where the heating cycle denotes that the Nitinol is in the state of heating from low temperature martensite to high temperature austenite, and vice versa for the cooling cycle; and TMCT (c) at 31.338 kHz.

(MKF115, BINDER) as the mechanism for applying controlled temperature functions. Transducers were placed on a polyurethane foam inside the climate chamber to establish boundary conditions as close to free-free as is physically practical. The resonance frequency and electrical impedance of the first longitudinal mode for both NMCT and TMCT were measured by sweeping through a designated frequency range at $0.5V_{RMS}$. All data were measured within a −40 °C to 60 °C temperature window, to capture all phase transitions of Nitinol as suggested through the DSC results shown in Fig. 1. The temperature step interval was set as 5 °C. The temperature was stabilised at each step for 10 minutes, to ensure that the temperature of each transducer equilibrated with the environment and was homogeneous through the device. Temperature was continuously and consistently monitored throughout.

In an ultrasonic system, the temperature of the device and the applied voltage directly influence the dynamic properties, such as resonance frequency and impedance. The hypothesis here is that the material behaviours unique to shape memory materials, and nonlinearities, associated with the Nitinol in the NMCT will interact differently with the expected softening behaviours associated with the PZT stack, as temperature and voltage change, for the NMCT compared to the titanium based TMCT. To quantify this, the temperature–voltage relationship was assessed by monitoring the dynamic properties of the transducers for different excitation voltages when the transducer temperature is stable. In each case, the resonance frequency, electrical impedance, and power are obtained by a driver (Ultrasonic Driver, PiezoDrive) which was connected externally to the transducers inside the climate chamber. The phase tracking function of the ultrasonic driver ensures that the transducers operate at their resonance frequency. To study the potential of the NMCT as a suitable candidate of power ultrasonic device for practical application, the vibration amplitude was obtained using a function generator (33210A, Keysight Technologies) and a signal amplifier (HFVA-62). Each transducer was excited using sinusoidal signals with voltages from $10V_{RMS}$ to $50V_{RMS}$, using a burst time interval of 3 seconds to minimise self-heating within the transducer where possible. By using a 1D LDV system (OFV-303, Polytec), the vibration amplitude of the first longitudinal mode is then collected.

Furthermore, the dynamics of the NMCT and TMCT were investigated using a combination of the ultrasonic driver, 1D LDV and a thermal imager (TM160, Micro-Epsilon). The self-heating phenomenon is caused by electric current forming in the PZT materials, thus generating Joule heating due to electrical impedance. This is particularly prominent in continuous driving conditions, which is common in power ultrasonics [39]. It was not practical to conduct this experiment below ambient temperature given the operating requirements of the measurement instruments, and so only vibration amplitude results for the 25 °C to 60 °C temperature range have been acquired.

3. Results and discussion

3.1. Measurements at static temperature

Before the experiment is conducted, the phase of the Nitinol material must be reset, ensuring the initial phase at the starting temperature is accurately known. This is because, due to its hysteretic nature, the phase microstructure of Nitinol can exist as either martensitic or austenitic, depending on whether a heating or cooling cycle is applied. This was done by using the aerosol freeze spray to cool the NMCT to −40 °C for 10 min and then gradually heat in ambient conditions until it returned to room temperature (20 °C). According to Fig. 1, the initial phase of Nitinol is a combination of martensite and austenite, because A_f has not yet been passed. The experiment includes three temperature functions to realise a heating-cooling loop: (1) heating the transducers from room temperature to 60 °C; (2) cooling the transducers from 60 °C to −40 °C; and (3) heating the transducers from −40 °C to room temperature. The first set of analyses aimed to evaluate the influence of static temperatures on NMCT dynamic properties, with particular focus on the resonance frequency. Resonance frequency results for the NMCT and TMCT in their first longitudinal mode with respect to temperature are shown in Fig. 6, extracted from the series resonance from EIA in each case.

The results show that the resonance frequencies of the TMCT monotonically decrease in the heating cycle, but increase in the cooling cycle. The experiment was conducted neglecting electrical losses, such dielectric loss and piezoelectric loss [40], with low excitation. Therefore, the resonance frequency differences are primarily contributed by the thermal softening of PZ26 elastic properties, especially c_{33} for longitudinal modes, and are partially influenced by the thermoelasticity. By contrast, the resonance frequencies of the NMCT do not exhibit this monotonical change across the heating-cooling loop. What is noticeable, is that there is a stability of resonance frequency at temperatures approximately higher than 20 °C and 10 °C in the heating and cooling cycles, respectively. The cause of this phenomenon can be attributed to the heat-hardening of Nitinol compensating for the heat-softening of the PZT.

In order to assess the resonance stability quantitatively, a half-power bandwidth superimposing technique is used. The half-power bandwidth is a measure of transducer performance in the frequency domain. Driving the transducer at any frequency inside the band, its power falls no lower than half of the peak value. Accordingly, it is acceptable in this study for NMCT and TMCT working in the half-power bandwidth. By superimposing bandwidth at two adjacent temperatures, the frequency range that satisfies driving at both temperatures can be obtained. Similarly, the superimposition can be undertaken across the entire temperature range, thus allowing measurement across a sufficiently wide heating-cooling loop. As shown in Fig. 6, the background of the figure shows the number of superimpositions corresponding to the right-side colour bar. The maximum superimpositions of NMCT and TMCT are 15 and 8, respectively. This interestingly implies that the NMCT could be driven reliably throughout the frequency band between 29.609 kHz to 29.651 kHz within temperature ranges of 20 °C to 50 °C and 10 °C to 45 °C in the heating and cooling cycles, respectively. Comparing to results of the TMCT, the NMCT shows a prominent resonance stability. It should be noted that this significant observation applies to the case including elastic loss only.

As shown in Fig. 7, electrical impedance results of NMCT and TMCT both exhibit strong temperature dependence. The impedance of TMCT increases and decreases during heating and cooling cycles, respectively. However, NMCT shows minimal variations within the temperature range from −40 °C to 25 °C. Above this range, NMCT's impedance

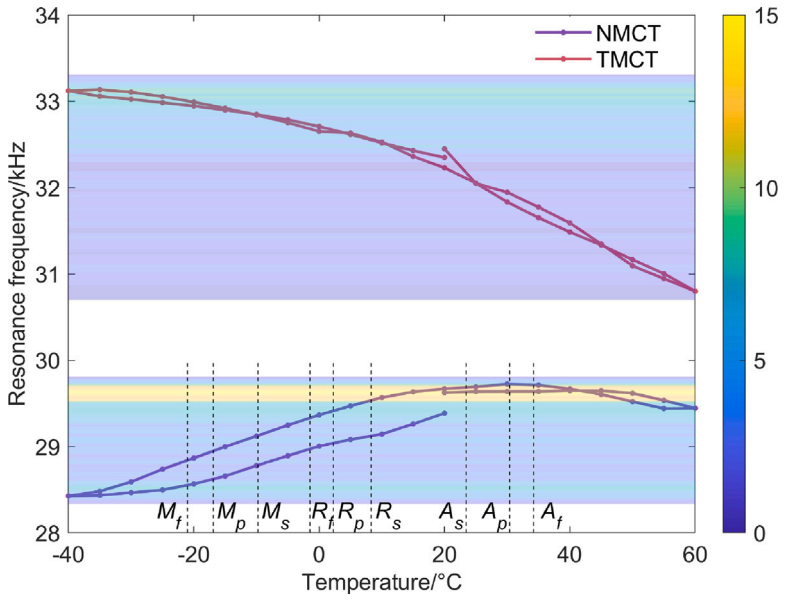

Fig. 6. Resonance frequencies of the NMCT and TMCT under the static temperature condition for the first longitudinal mode within a −40 °C to 60 °C temperature window. The background colour illustrates the number of superimpositions of half-power bandwidths across the temperature window for both transducers, as reference to the right-side colour bar.

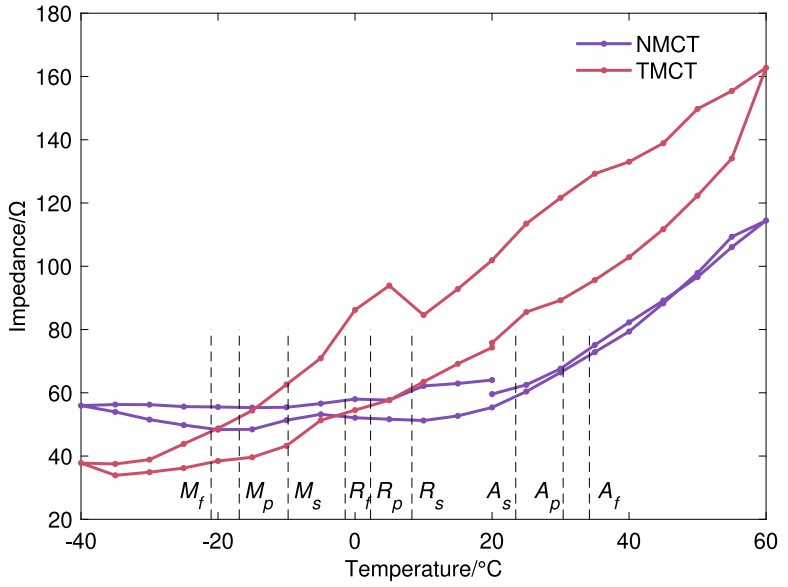

Fig. 7. Electrical impedance results of NMCT and TMCT with respect to temperature.

undergoes similar rates of change to that of TMCT. Statistically, the smaller range of the data set of NMCT impedance compared to TMCT confirms that the former has a lower spread in the data, and thus is less sensitive to temperature. Moreover, phase transition temperatures in Fig. 1 broadly align with the patterns in the data trends for the NMCT. This indicates the phase transitions influence the electrical properties in a transducer. It is worth noting that the larger area enclosed by curves of TMCT results indicate a higher hysteresis than that of the NMCT, and in general, it is evident that Nitinol phase transitions affect transducer electrical properties.

From here, dynamic properties including antiresonance frequency, half-power bandwidth, quality factor, and electromechanical coupling coefficient, are compared. As shown in Fig. 8(a) and (b), antiresonance frequency and half-power bandwidth results are consistent with the trends shown in Figs. 6 and 7, respectively. Both half-power bandwidth and quality factor are indicators of the resonance behaviour of an ultrasonic transducer in an underdamped condition. Since NMCT has a wider bandwidth and a lower quality factor than TMCT through the heating-cooling loop in Fig. 8(b) and (c), NMCT has greater damping. It shows significant potential for NMCT to be applied into sensing applications, in addition to power ultrasonic applications. Another indicator for analysing the dynamics response is the electromechanical coupling coefficient which is a measure of the fraction of electrical energy that can be converted into mechanical energy and vice versa in an ultrasonic transducer system. The electromechanical coupling coefficient can be obtained using IEEE 176-1987 [41], as shown in (1).

$$(k_{33}^{l})^2 = \frac{\pi f_s}{2f_p} tan\left(\frac{\pi(f_p - f_s)}{2f_p}\right) \tag{1}$$

Here, k_{33}^{l} is the electromechanical coupling coefficient, f_s is the frequency of maximum conductance, and f_p is the frequency of maximum resistance. In Fig. 8(d), the electromechanical coupling coefficient of

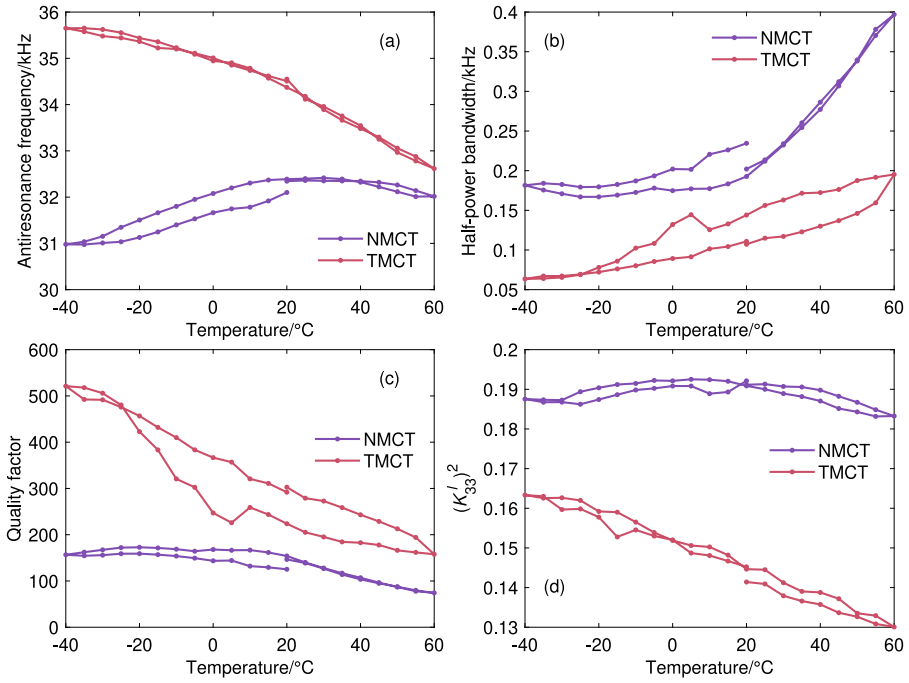

Fig. 8. (a) Antiresonance frequency, (b) half-power bandwidth, (c) quality factor, and (d) electromechanical coupling coefficient of the NMCT and TMCT with respect to temperature.

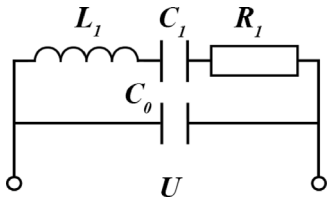

Fig. 9. Unloaded BVD model diagram.

NMCT is almost constant over the entire temperature window, while that of TMCT is decreased with an increasing temperature. This implies that the resonance stability exists in the electromechanical coupling coefficient of NMCT. Thus, the incorporation of Nitinol enables a higher and stable energy conversion in the transducer.

A clearer understanding of the dynamic responses for the NMCT can be achieved by considering the unloaded conventional Butterworth Van Dyke (BVD) equivalent circuit model as shown in Fig. 9 [42]. This model describes the connection between mechanical and electrical properties for an ultrasonic transducer. In the equivalent circuit diagram, C_0 is the electrical static capacitance, C_1 is the mechanical equivalent capacitance, L_1 is the mechanical equivalent inductance, and R_1 is the mechanical equivalent resistance.

Based on the BVD model, the first parameter that can be obtained from experimental impedance spectra is R_1. At the resonance frequency, where its phase is zero, the transducer becomes a transient and purely resistive system. Therefore, R_1 equals the resonance impedance, and the experimentally measured impedance at an off-resonance frequency is the sum of the impedance for C_0 and C_1. Relations of components in the BVD model are described through (2) to (4).

$$Q = \frac{1}{2\pi f_r R_1 C_1} \tag{2}$$

$$L_1 = \frac{1}{(2\pi f_r)^2 C_1} \tag{3}$$

$$Z_{off} = C_0 + C_1 \tag{4}$$

Here, Q is the quality factor, f_r is the resonance frequency, and Z_{off} is the impedance at the off-resonance frequency. Calculated results for C_0, C_1, L_1, and R_1 with respect to different temperatures are shown in Fig. 10.

C_0 denotes the electrical capacitance of the transducer, which is defined by intrinsic electrical properties of PZT. As shown in Fig. 10(a), NMCT capacitance remains higher than those of the TMCT across the temperature window, though in the same order of magnitude. The energy stored in the PZT is the product of C_0 and square of the voltage applied, divided by two. From this, it is evident that the NMCT can store more electrical energy for a given applied voltage. A practical method to analyse the results in Fig. 10(b), (c), and (d) is to describe the mechanical system through the impedance analogy [43]. Equivalent mechanical parameters C_1, L_1, and R_1 represent compliance, mass inertia, damping, respectively [44]. The magnitude of C_1 in Fig. 10(b) increases with a rise in temperature, and vice versa. This indicates that TMCT's compliance exhibits a similar variation with C_1, as its stiffness is the inverse of compliance, aligning with the thermal softening effect of PZT in Fig. 6. However, the C_1 magnitude of the NMCT is effectively constant, showing that the change in Nitinol stiffness contributes to the compensation of the softening of the PZT. Besides, L_1 in Fig. 10(c) suggests that the mass inertia of the TMCT decreases with a rise in temperature, and vice versa. However, the mass inertia of NMCT is generally constant, and lower than that of the TMCT. This can be explained by the fact that the TMCT can readily achieve higher vibration velocities than the NMCT, and it can be more significantly influenced by variations in this temperature window. In Fig. 10(d), the R_1 analogised damping of both the NMCT and the TMCT increases with a rise in temperature, which corresponds to the half-power bandwidth shown in Fig. 8(b). The hysteresis of mass, compliance, and damping can explain the existence of impedance and resonance frequency hysteresis for both the NMCT and the TMCT.

3.2. Measurements at static temperature-voltage

To introduce dielectric loss and piezoelectric loss effects, NMCT and TMCT are measured from $10V_{RMS}$ to 50 V_{RMS} in a defined heating-cooling cycle. The resonance frequencies of the NMCT and TMCT are

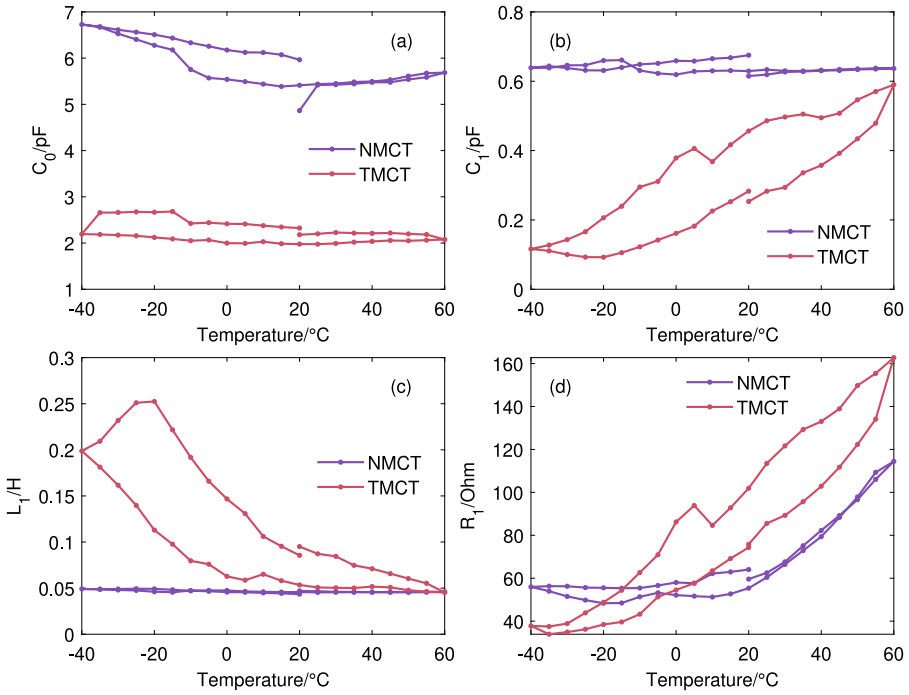

Fig. 10. Calculated C_0 (a), C_1 (b), L_1 (c), and R_1 (d) results from the BVD model.

shown in Fig. 11(a) as functions of both voltage and temperature. Multiple factors, including fatigue of PZT materials and slight temperature differences, can be attributed to the jump phenomenon of transducers at room temperature in the heating cycle. Changes of resonance frequency in the NMCT and TMCT follow a similar trend to that exhibited in Fig. 6, across all applied voltage levels. In general, the higher the voltage applied, the lower the frequency of NMCT and TMCT, which is a nonlinear softening behaviour of ultrasonic transducers that has been widely reported in the literature over many years [45,46]. Specific to the NMCT, resonance stability is detected at temperatures around ambient room temperature. Utilising the half-power bandwidth superimposition method described earlier, the quantified resonance stability is shown in Fig. 11(b). Coloured areas represent the frequency band and maximum temperature window that generated the associated level of resonance stability. As voltage increases, both the width of the frequency band and the temperature range rise. Comparing the results in Fig. 6 and those for $10V_{RMS}$ in Fig. 11(b), stability was reduced, likely due to the introduction of electrical losses. However, stability was enhanced with an increase in applied voltage level. It should be noted that the stabilised temperature range in the cooling loop is significantly wider than that in the heating loop. Therefore, the austenite in the Nitinol microstructure appears to more favourably induce resonance stability, compared to the microstructure comprising a mix of austenite and martensite. It is also important to note that within the stabilised temperature window, the variation of resonance frequencies is within 1%.

The electrical impedance of both the NMCT and TMCT are shown to rise with increasing voltage, as shown in Fig. 12. Comparing these results to those shown in Fig. 7, there appears to be negligible hysteresis, likely due to the electrical losses in the PZT for rising applied voltage level. The electrical impedance of the NMCT is a function of temperature in the voltage range from $10V_{RMS}$ to $50V_{RMS}$, when the temperature is above 15 °C, but generally stable below this temperature. Additionally, the results also show the NMCT has a lower impedance spread than that of TMCT. Therefore, the NMCT demonstrates higher electrical stability than the TMCT.

This analysis can be extended to considering comparisons for antiresonance frequency, half-power bandwidth, quality factor, and electromechanical coupling coefficient. This data is summarised in Fig. 13, and in general it is evident that the changes in these properties with temperature are consistent with the results presented in Fig. 8, irrespective of applied voltage level. Antiresonance frequencies at different voltages, as shown in Fig. 13(a), exhibit resonance stability in the data around the room temperature. Thus, the phase transition of the Nitinol affects the resonance and antiresonance frequencies simultaneously. As shown in Fig. 13(b), the NMCT has wider half-power bandwidth overall and higher spread of data at higher voltage excitation levels. This likely indicates that the NMCT has higher mechanical damping which is more readily influenced by the applied voltage level. Moreover, the quality factor of the NMCT in Fig. 13(c) demonstrates that the damping of the NMCT system is a function of voltage, resulting in higher energy loss, and there appears to be a more significant reduction in quality factor for the TMCT compared to the NMCT for given applied voltage increases. Furthermore, it can be seen in Fig. 13(d) that electromechanical coefficients of the NMCT and TMCT are functions of both voltage and temperature. Whilst the electromechanical coefficient of the TMCT appears to be relatively independent of applied voltage, unlike for the NMCT, there is a general stability of the electromechanical coefficient across the specified temperature window (heating or cooling) which is not detected for the TMCT, which progressively reduced as temperature rises. Although the electromechanical coefficient is generally stable for the NMCT, there are slight increases in both cycles, unlike the phenomenon depicted in Fig. 8(d). Both hysteresis and temperature dependence can be attributed to variations in elastic and electrical losses in the system, under different applied voltages.

Next, the load power response of both the TMCT and NMCT were measured, and these are shown in Fig. 14. On the right side of the power cut-off line, the load power of the NMCT is shown to significantly reduce with temperature. However, on the left side of the line, the power remains constant at different voltages and is reversible. This is a notably different behaviour compared to the TMCT load power results, which all exhibit a general decrease as temperature rises, as shown in Fig. 14(b). This verifies that the NMCT's electrical properties also exhibit a degree of stability. As voltage increases, the range of steady power gradually narrows, and the temperature window for stability is reduced. When the device is operated on the left-hand side of the cut-off line, the approximately constant load power and electromechanical

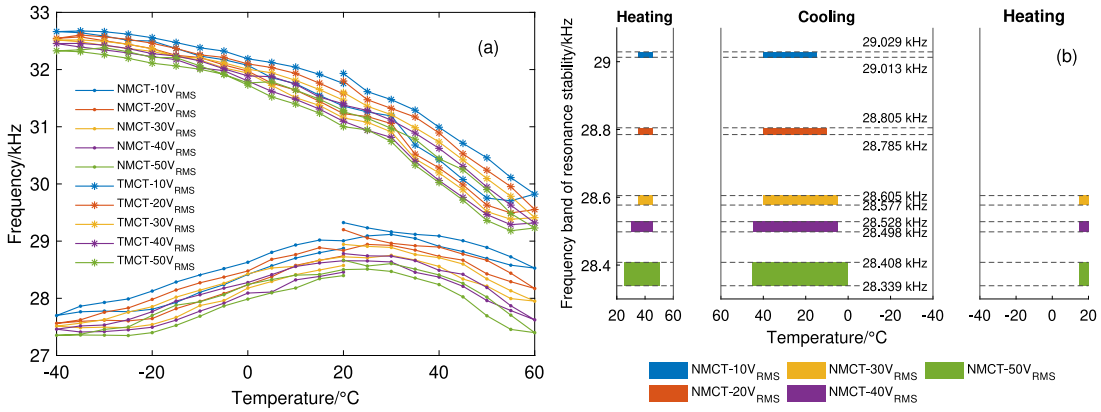

Fig. 11. (a) Resonance frequency and (b) the frequency band of resonance stability for the NMCT and TMCT under the static temperature-voltage condition for the first longitudinal mode within a −40 °C to 60 °C temperature window, and applied voltages of $10V_{RMS}$ to $50V_{RMS}$.

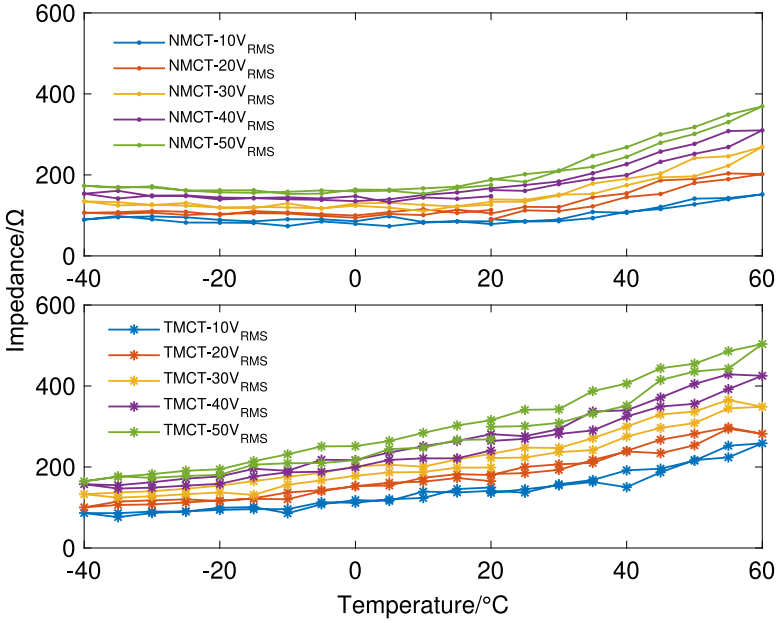

Fig. 12. Impedance magnitudes of the NMCT and TMCT under the static temperature-voltage condition for the first longitudinal mode within a −40 °C to 60 °C temperature window, and applied voltages of $10V_{RMS}$ to $50V_{RMS}$.

coupling coefficient (Fig. 13(d)) means power tracking is not required. This electrical stability can be potentially applied to cold working conditions, such as ultrasonic de-icing.

The vibration amplitude responses of the NMCT as functions of temperature were then measured for different applied voltages, and these results are shown in Fig. 15. There were practical limitations on the environments in which the LDV could be operated, and so this harmonic analysis process was only performed at room temperature. As described in Section 2.2, the NMCT incorporates Nitinol existing in one of two states at room temperature. This due to the hysteresis in the material, with differences depending on a heating or cooling cycle being applied. Measurements were made with Nitinol in each microstructure, with voltage increased from $10V_{RMS}$ to $50V_{RMS}$ in $10V_{RMS}$ steps, then decreased back to $10V_{RMS}$.

In general, there is a high level of consistency and similarity between the data from both cycles, with nonlinear softening consistent with behaviours reported in other research of Langevin transducer dynamics [47,48], in addition to the nonlinear jump phenomenon [49]. As the applied voltage rises, the maximum displacement amplitude is higher for the NMCT after the cooling cycle (at almost identical resonance frequencies). Slight differences in impedance contribute to differences in amplitude, but also the microstructure of the Nitinol will have an influence. In addition, the red dashed line in Fig. 15 indicates the hysteresis of the rising and falling voltage, which is consistent with the polarisation vs electrical (P-E) hysteresis loop of PZT material due to internal field bias [50]. The NMCT in the heating cycle exhibits a more prominent hysteresis at higher voltages, which suggests that the NMCT in this condition has lower polarisation dissipation energy and less remnant polarisation.

3.3. Influence of self-heating on dynamics

The experimental results detailed so far were obtained using static temperature conditions. However, in practical applications, the thermal conditions generated by Joule heating in the PZT can induce an unevenly distributed temperature field, or self-heating, in the transducer. Therefore, quantifying and accounting for self-heating is important for studying the resonance stability of the NMCT. The self-heating was only explored for the NMCT in the cooling cycle, given its higher amplitude and lower hysteresis than that of the heating cycle, as shown in Fig. 15. Here, the transducers are operated continuously until either the PZT stack temperature reaches 60 °C or the elapsed measurement time is

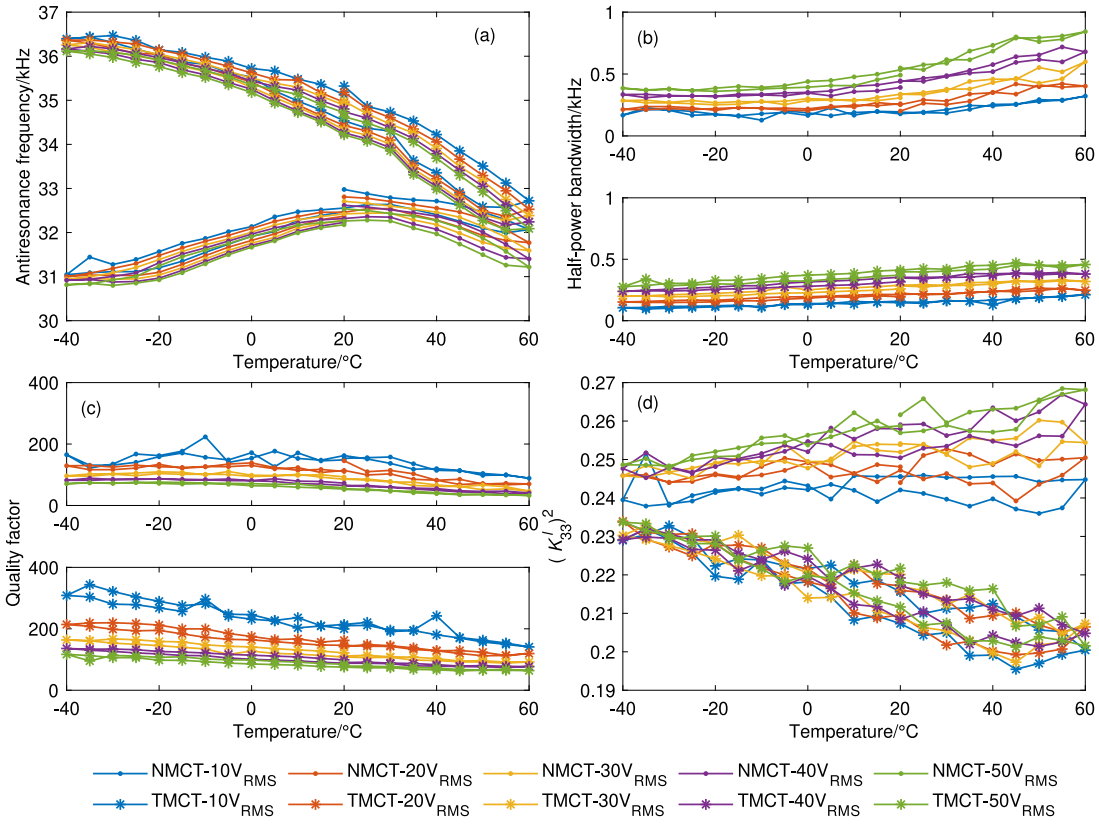

Fig. 13. (a) Antiresonance frequency, (b) half-power bandwidth, (c) quality factor, and (d) electromechanical coupling factor results for the NMCT and TMCT under the static temperature-voltage condition for the first longitudinal mode within a −40 °C to 60 °C temperature window, and applied voltages of $10V_{RMS}$ to $50V_{RMS}$.

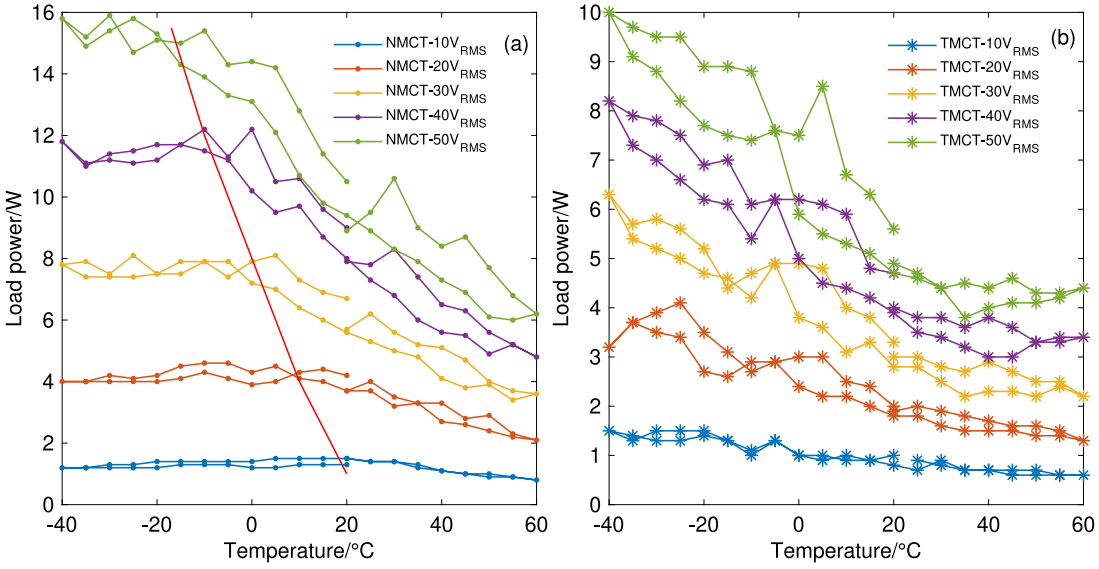

Fig. 14. Load power results of (a) the NMCT and (b) the TMCT under the static temperature-voltage condition for the first longitudinal mode within a −40 °C to 60 °C temperature window, and applied voltages of $10V_{RMS}$ to $50V_{RMS}$.

300 s. The measurements for both transducers are shown in Fig. 16, which are recorded using a thermal imager. It should be noted that during the experiment, only the temperature changes of the two PZT stacks and the middle mass are included, given the negligible changes in temperature of the end-masses. It is also clear that the PZT stacks generally reach higher temperatures than the middle mass.

The frequency as a function of time for the transducers are shown in Fig. 17(a), it appears that the resonance frequency of NMCT can be stabilised within relatively short time spans when the voltage is lower than $50V_{RMS}$. The frequency difference at times from 4s to 104s at $20V_{RMS}$ is only 10 Hz, which is indicative of a significant resonance stability performance. However, the resonance frequency of the TMCT as shown in Fig. 17(b) decreases as the time increases, regardless of the voltage excitation level. Interestingly, the impedance of NMCT and TMCT exhibit almost the same behaviour, as shown in Fig. 17(c) and (d). This may be because the temperature of the Nitinol is much lower

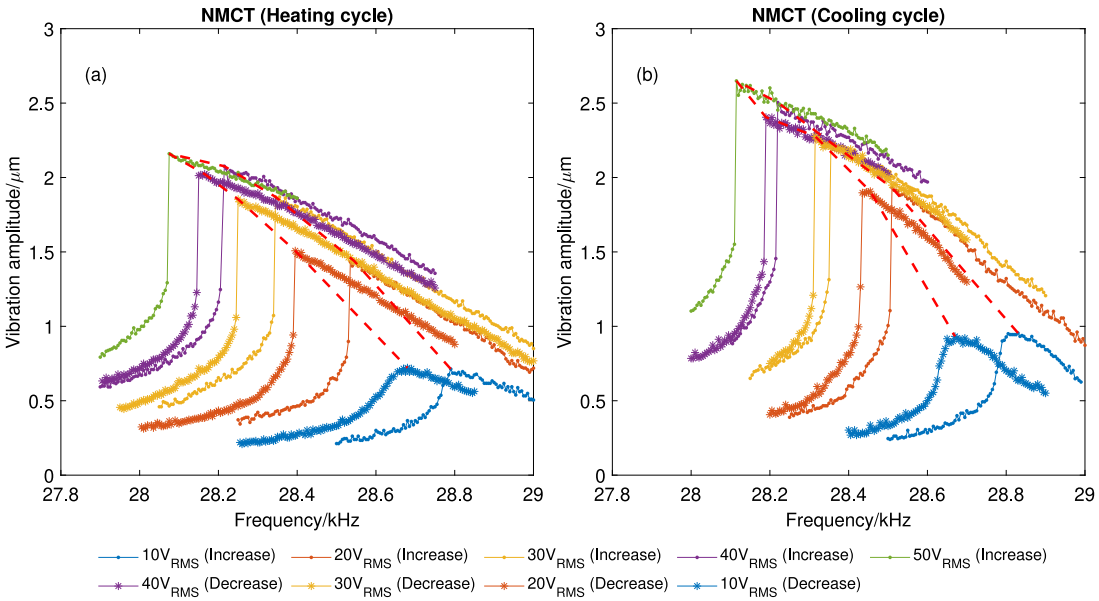

Fig. 15. Vibration amplitude spectra of the NMCT from $10V_{RMS}$ to $50V_{RMS}$ after (a) the heating cycle (a) and (b) the cooling cycle.

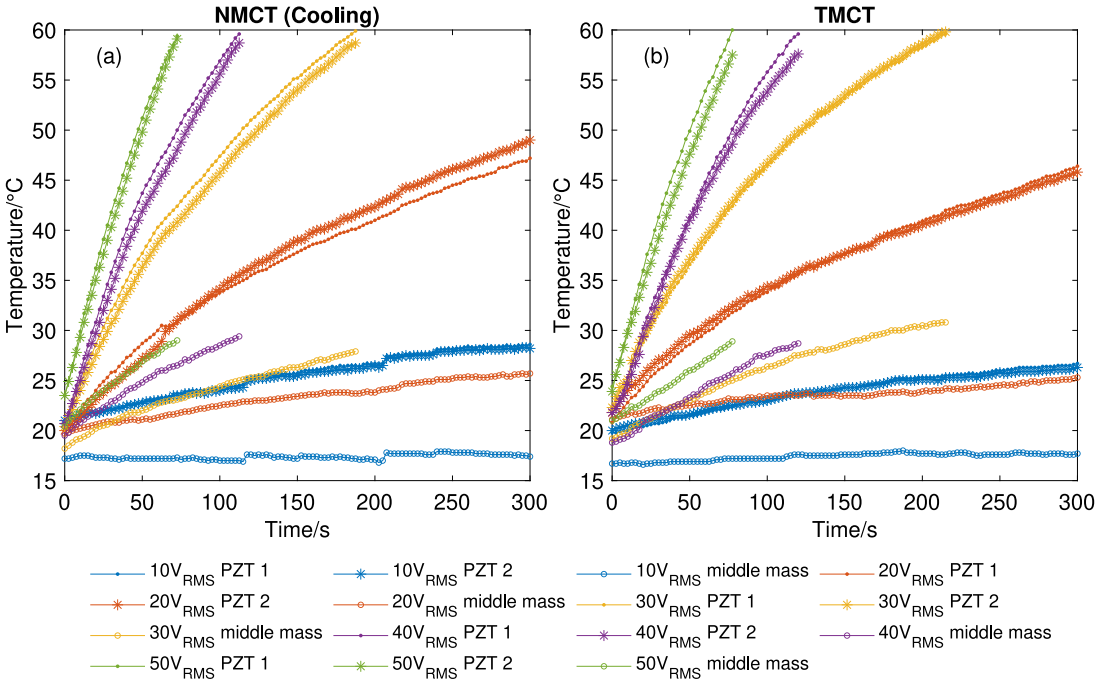

Fig. 16. Temperature as a function of time of the two PZT stacks and the middle mass for (a) the NMCT and (b) the TMCT under self-heating conditions, and applied voltages of $10V_{RMS}$ to $50V_{RMS}$.

than that of PZT stacks, which means that Nitinol cannot significantly influence the transducer's electrical properties. Moreover, both the NMCT and TMCT exhibit similar current RMS and load power responses as shown in Fig. 17(e), (f), (g), and (h), suggesting that Nitinol does not have notable influence on the dynamics from self-heating.

As shown in Fig. 18(a) to (h), the temperatures of the PZT stacks and the middle mass of the NMCT have been monitored, where the PZT stacks are consistently observed to be the hottest. Although the temperature of the Nitinol middle mass does increase, it is significantly lower than that of the PZT stacks. To investigate further, the temperature of the PZT was used as a reference, where temperature was adjusted in intervals of 5 °C as the NMCT was driven in a continuous mode from $10V_{RMS}$ to $50V_{RMS}$ before decreasing back to $10V_{RMS}$, in steps of $10V_{RMS}$. In Fig. 18(i), vibration amplitude results are displayed with respect to resonance frequency, PZT temperature, and excitation voltage, which is indicated by the coloured areas. As the voltage increases, the vibration amplitudes between 25 °C and 45 °C remain generally stable, whereas the difference between the NMCT at 45 °C and 50 °C becomes more pronounced. This means that despite the non-uniform temperature distribution in the NMCT, resonance stability still exists in its vibration amplitude, and the applicable temperature range is larger compared to Fig. 11(b). There appear to be optimal conditions to drive the NMCT, dependent on the transducer assembly. It is worth noting that under self-heating conditions, the vibration amplitude associated with a particular excitation voltage remains at a similar level between 25 °C and 45 °C. Overall, this phenomenon

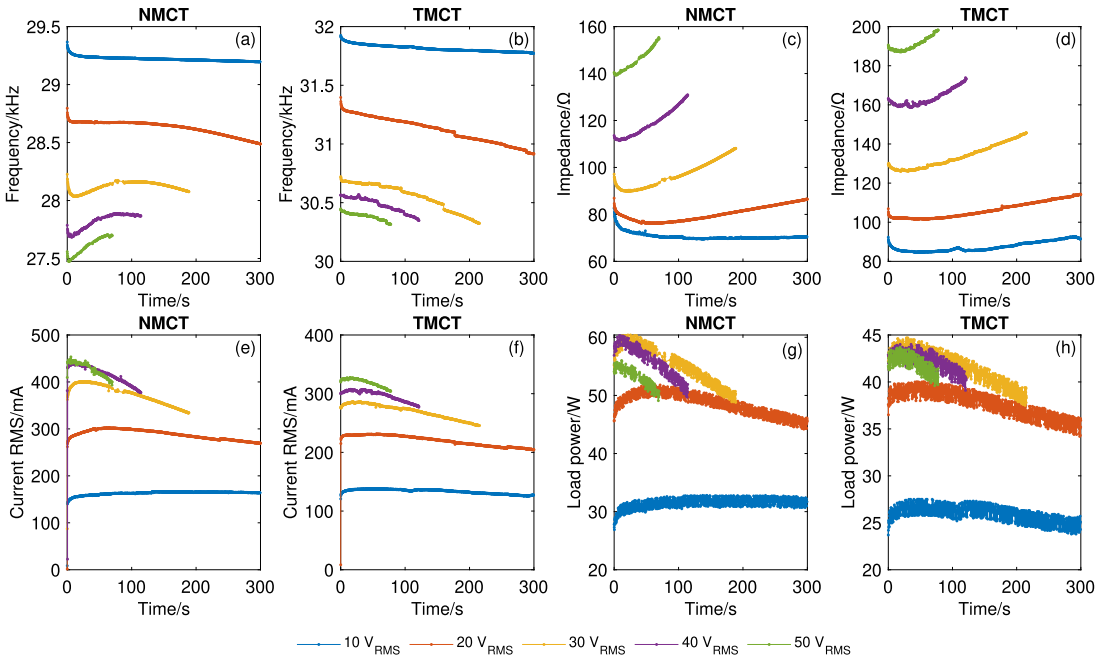

Fig. 17. Resonance frequency (a) and (b), impedance (c) and (d), current RMS (e) and (f), and load results (g) and (h) of the NMCT and TMCT under self-heating conditions, and applied voltages of $10V_{RMS}$ to $50V_{RMS}$.

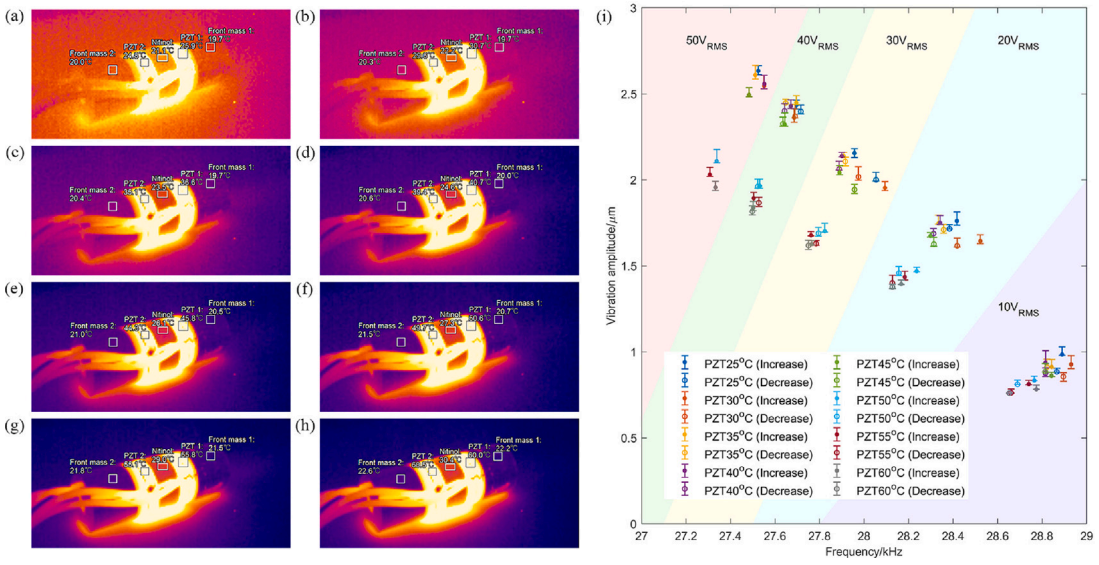

Fig. 18. Thermal imaging maps showing self-heating in the NMCT, including PZT stack temperatures of (a) 25 °C, (b) 30 °C, (c) 35 °C, (d) 40 °C, (e) 45 °C, (f) 50 °C, (g) 55 °C, and (h) 60 °C, and (i) vibration amplitudes with respect to resonance frequency, PZT stack temperature, and excitation voltage (coloured areas).

reveals the potential of the NMCT being applied to power ultrasonic applications utilising continuous mode excitation at higher voltage levels, ensuring a stabilised output vibration amplitude within the 20 °C to 45 °C temperature range.

4. Conclusion

Comprehensive research for the NMCT is presented in this study, aiming to fulfil the resonance stability in an ultrasonic transducer by incorporating Nitinol. The phase transitions of Nitinol have been characterised by DSC. Based on the structural acoustic impedance, NMCT and TMCT were designed and manufactured. In order to research the static temperature influence on NMCT dynamics firstly, comparisons were completed between the NMCT and TMCT without considering electrical losses. The results demonstrate that the resonance stability exists in typical temperature ranges for resonance frequency, antiresonance frequency, and electromechanical coupling coefficient. According to the BVD model and impedance analogy, variations of structural properties of NMCT and TMCT were estimated. Secondly, the introduction of electrical losses was performed by testing NMCT and TMCT in the same temperature function but across $10V_{RMS}$ to $50V_{RMS}$ excitations. In fact, the resonance stability was reduced by electrical losses. Interestingly, the higher the voltage, the wider the temperature and frequency ranges for the stability phenomenon. Comparing to the TMCT, the impedance and half-power bandwidth of NMCT are more sensitive to voltage. It is worth noting that the existence of the power cut-off line in the NMCT demonstrates that load power is not a function of temperature at low temperatures. Vibration amplitude

at room temperature for the NMCT with austenitic Nitinol in the cooling cycle is higher with lower hysteresis than for a combination of martensite and austenite in the heating cycle. Finally, the self-heating experiment shows the NMCT exhibits resonance stability of the resonance frequency and vibration amplitude with unevenly distributed temperature fields. This makes especially suitable for power ultrasonic applications.

CRediT authorship contribution statement

Yuchen Liu: Conceptualization, Methodology, Validation, Investigation, Software, Visualization, Writing – original draft. **Mahshid Hafezi:** Investigation, Writing – review & editing. **Andrew Feeney:** Writing – review & editing, Supervision, Project administration, Funding acquisition.

Declaration of competing interest

The authors declare that they have no known competing financial interests or personal relationships that could have appeared to influence the work reported in this paper.

Data availability

Data will be made available on request.

Acknowledgements

This work was supported by the Engineering and Physical Sciences Research Council, United Kingdom (Grant EP/V049658/1). We acknowledge the assistance from Dr Paul Barron for manufacturing the Nitinol ring and differential scanning calorimetry testing.

References

[1] T.-G. Park, D.-S. Jeong, M.-H. Kim, T.-K. Song, A study on the rotary-type ultrasonic motor using a longitudinal–torsional vibration converter, Mater. Chem. Phys. 98 (1) (2006) 1–4, http://dx.doi.org/10.1016/j.matchemphys.2004.09.049.

[2] F. Bejarano, A. Feeney, R. Wallace, H. Simpson, M. Lucas, An ultrasonic orthopaedic surgical device based on a cymbal transducer, Ultrasonics 72 (2016) 24–33, http://dx.doi.org/10.1016/j.ultras.2016.07.004.

[3] A. Mathieson, D.A. DeAngelis, Analysis of lead-free piezoceramic-based power ultrasonic transducers for wire bonding, IEEE Trans. Ultrason. Ferroelectr. Freq. Control 63 (1) (2015) 156–164, http://dx.doi.org/10.1109/TUFFC.2015.2496216.

[4] H. Al-Budairi, M. Lucas, P. Harkness, A design approach for longitudinal–torsional ultrasonic transducers, Sensors Actuators A 198 (2013) 99–106, http://dx.doi.org/10.1016/j.sna.2013.04.024.

[5] R. Georges Sabat, B.K. Mukherjee, W. Ren, G. Yang, Temperature dependence of the complete material coefficients matrix of soft and hard doped piezoelectric lead zirconate titanate ceramics, J. Appl. Phys. 101 (6) (2007) http://dx.doi.org/10.1063/1.2560441.

[6] K. Uchino, S. Hirose, Loss mechanisms in piezoelectrics: how to measure different losses separately, IEEE Trans. Ultrason. Ferroelectr. Freq. Control 48 (1) (2001) 307–321, http://dx.doi.org/10.1109/58.896144.

[7] M.H. Amini, A.N. Sinclair, T.W. Coyle, A new high-temperature ultrasonic transducer for continuous inspection, IEEE Trans. Ultrason. Ferroelectr. Freq. Control 63 (3) (2016) 448–455, http://dx.doi.org/10.1109/TUFFC.2016.2519348.

[8] T. Wang, Q. Quan, D. Tang, Z. Yang, J. Huang, F. Guo, L. Meng, Z. Zhao, Z. Deng, Effect of hyperthermal cryogenic environments on the performance of piezoelectric transducer, Appl. Therm. Eng. 193 (2021) 116725, http://dx.doi.org/10.1016/j.applthermaleng.2021.116725.

[9] D. Yamaguchi, T. Kanda, K. Suzumori, An ultrasonic motor for cryogenic temperature using bolt-clamped Langevin-type transducer, Sensors Actuators A 184 (2012) 134–140, http://dx.doi.org/10.1016/j.sna.2012.06.024.

[10] Y. Yao, Y. Pan, S. Liu, Study on heat pipe heat dissipation of high-power ultrasonic transducer, Ultrasonics 120 (2022) 106654, http://dx.doi.org/10.1016/j.ultras.2021.106654.

[11] J. Kim, J. Lee, Acoustic and thermal characterization of therapeutic ultrasonic langevin transducers under continuous-and pulsed wave excitations, Sensors 22 (22) (2022) 9006, http://dx.doi.org/10.3390/s22229006.

[12] Z. Wu, W. Liu, Z. Tong, Y. Cai, C. Sun, L. Lou, Tuning characteristics of AlN-based piezoelectric micromachined ultrasonic transducers using DC bias voltage, IEEE Trans. Electron Devices 69 (2) (2022) 729–735, http://dx.doi.org/10.1109/TED.2021.3137766.

[13] A. Feeney, M. Lucas, A comparison of two configurations for a dual-resonance cymbal transducer, IEEE Trans. Ultrason. Ferroelectr. Freq. Control 65 (3) (2018) 489–496, http://dx.doi.org/10.1109/TUFFC.2018.2793310.

[14] A. Feeney, M. Lucas, Differential scanning calorimetry of superelastic Nitinol for tunable cymbal transducers, J. Intell. Mater. Syst. Struct. 27 (10) (2016) 1376–1387, http://dx.doi.org/10.1177/1045389X15591383.

[15] A. Feeney, M. Lucas, Smart cymbal transducers with nitinol end caps tunable to multiple operating frequencies, IEEE Trans. Ultrason. Ferroelectr. Freq. Control 61 (10) (2014) 1709–1719, http://dx.doi.org/10.1109/TUFFC.2013.006231.

[16] T. Duerig, A. Pelton, D. Stöckel, An overview of nitinol medical applications, Mater. Sci. Eng. A 273 (1999) 149–160, http://dx.doi.org/10.1016/S0921-5093(99)00294-4.

[17] M. Hassan, F. Scarpa, M. Ruzzene, N. Mohammed, Smart shape memory alloy chiral honeycomb, Mater. Sci. Eng. A 481 (2008) 654–657, http://dx.doi.org/10.1016/j.msea.2006.10.219.

[18] J.M. Jani, M. Leary, A. Subic, M.A. Gibson, A review of shape memory alloy research, applications and opportunities, Mater. Des. (1980-2015) 56 (2014) 1078–1113, http://dx.doi.org/10.1016/j.matdes.2013.11.084.

[19] Y. Liu, H. Xiang, Apparent modulus of elasticity of near-equiatomic NiTi, J. Alloys Compd. 270 (1–2) (1998) 154–159, http://dx.doi.org/10.1016/S0925-8388(98)00500-3.

[20] K. Suresh, D. Lahiri, A. Agarwal, S. Suwas, Microstructure dependent elastic modulus variation in NiTi shape memory alloy, J. Alloys Compd. 633 (2015) 71–74, http://dx.doi.org/10.1016/j.jallcom.2015.01.301.

[21] P. Šittner, L. Heller, J. Pilch, C. Curfs, T. Alonso, D. Favier, Young's modulus of austenite and martensite phases in superelastic NiTi wires, J. Mater. Eng. Perform. 23 (2014) 2303–2314, http://dx.doi.org/10.1007/s11665-014-0976-x.

[22] O. Benafan, R. Noebe, S. Padula Ii, A. Garg, B. Clausen, S. Vogel, R. Vaidyanathan, Temperature dependent deformation of the B2 austenite phase of a NiTi shape memory alloy, Int. J. Plast. 51 (2013) 103–121, http://dx.doi.org/10.1016/j.ijplas.2013.06.003.

[23] G. Laplanche, J. Pfetzing-Micklich, G. Eggeler, Orientation dependence of stress-induced martensite formation during nanoindentation in NiTi shape memory alloys, Acta Mater. 68 (2014) 19–31, http://dx.doi.org/10.1016/j.actamat.2014.01.006.

[24] M. Thomasová, P. Sedlák, H. Seiner, M. Janovská, M. Kabla, D. Shilo, M. Landa, Young's moduli of sputter-deposited NiTi films determined by resonant ultrasound spectroscopy: Austenite, R-phase, and martensite, Scr. Mater. 101 (2015) 24–27, http://dx.doi.org/10.1016/j.scriptamat.2015.01.00.

[25] S. Lin, C. Xu, Analysis of the sandwich ultrasonic transducer with two sets of piezoelectric elements, Smart Mater. Struct. 17 (6) (2008) 065008, http://dx.doi.org/10.1088/0964-1726/17/6/065008.

[26] J.W. Mwangi, V.D. Bui, K. Thuesing, S. Hahn, M.F.-X. Wagner, A. Schubert, Characterization of the arcing phenomenon in micro-EDM and its effect on key mechanical properties of medical-grade nitinol, J. Mater Process. Technol. 275 (2020) 116334, http://dx.doi.org/10.1016/j.jmatprotec.2019.116334.

[27] M. Thomasová, H. Seiner, P. Sedlák, M. Frost, M. Ševčík, I. Szurman, R. Kocich, J. Drahokoupil, P. Šittner, M. Landa, Evolution of macroscopic elastic moduli of martensitic polycrystalline NiTi and NiTiCu shape memory alloys with pseudoplastic straining, Acta Mater. 123 (2017) 146–156, http://dx.doi.org/10.1016/j.actamat.2016.10.024.

[28] S. Rajagopalan, A. Little, M. Bourke, R. Vaidyanathan, Elastic modulus of shape-memory NiTi from in situ neutron diffraction during macroscopic loading, instrumented indentation, and extensometry, Appl. Phys. Lett. 86 (8) (2005) http://dx.doi.org/10.1063/1.1863437.

[29] M.F.-X. Wagner, Microstructural and mechanical challenges in biomedical NiTi, J. Phys.: Conf. Ser. 240 (1) (2010) 012004, http://dx.doi.org/10.1088/1742-6596/240/1/012004.

[30] Q. Mei, L. Zhang, K. Tsuchiya, H. Gao, T. Ohmura, K. Tsuzaki, Grain size dependence of the elastic modulus in nanostructured NiTi, Scr. Mater. 63 (10) (2010) 977–980, http://dx.doi.org/10.1016/j.scriptamat.2010.07.018.

[31] K. Chu, B. Wang, Q. Li, Y. Onuki, F. Ren, Grain size effect on the temperature-dependence of elastic modulus of nanocrystalline NiTi, J. Alloys Compd. 934 (2023) 167907, http://dx.doi.org/10.1016/j.jallcom.2022.167907.

[32] W. Theisen, A. Schuermann, Electro discharge machining of nickel–titanium shape memory alloys, Mater. Sci. Eng. A 378 (1–2) (2004) 200–204, http://dx.doi.org/10.1016/j.msea.2003.09.115.

[33] Y. Feng, J. Qiao, L. Li, Acoustic behavior of composites with gradient impedance, Mater. Des. 193 (2020) 108870, http://dx.doi.org/10.1016/j.matdes.2020.108870.

[34] T.R. Kelley, Lead-free versus PZT: Acoustic characterization of ultrasonic immersion transducers fabricated with lead-free NBT-BT piezoceramic, J. Eng. 2023 (6) (2023) e12282, http://dx.doi.org/10.1049/tje2.12282.

[35] I. Ibanez, B. Zeqiri, M. Hodnett, M. Frota, Cavitation-erosion measurements on engineering materials, Eng. Sci. Technol., Int. J. 23 (6) (2020) 1486–1498, http://dx.doi.org/10.1016/j.jestch.2020.06.001.

[36] A.A. Mohammed, S.M. Haris, M.Z. Nuawi, Utilizing Hilbert–Huang transform in detection some of mechanical properties of the refractory metals, Mech. Syst. Signal Process. 68–69 (2016) 449–461, http://dx.doi.org/10.1016/j.ymssp.2015.07.024.

[37] X. Wang, W. Xia, X. Wu, Y. Wei, C. Huang, In-situ investigation of dynamic deformation in NiTi shape memory alloys under laser induced shock, Mech. Mater. 114 (2017) 69–75, http://dx.doi.org/10.1016/j.mechmat.2017.06.009.

[38] H. Daneshpajooh, M. Choi, Y. Park, T. Scholehwar, E. Hennig, K. Uchino, Compressive stress effect on the loss mechanism in a soft piezoelectric Pb(Zr,Ti)O3, Rev. Sci. Instrum. (ISSN: 0034-6748) 90 (7) (2019) 075001, http://dx.doi.org/10.1063/1.5096905.

[39] A. Wellendorf, L. von Damnitz, A.W. Nuri, D. Anders, S. Trampnau, Determination of the temperature-dependent resonance behavior of ultrasonic transducers using the finite-element method, J. Vibr. Eng. Technol. (2023) 1–14, http://dx.doi.org/10.1007/s42417-023-00906-8.

[40] K. Uchino, Y. Zhuang, S.O. Ural, Loss determination methodology for a piezoelectric ceramic: new phenomenological theory and experimental proposals, J. Adv. Dielectr. 1 (01) (2011) 17–31, http://dx.doi.org/10.1142/S2010135X11000033.

[41] IEEE standard on piezoelectricity, ANSI/IEEE Std 176-1987, 1988, http://dx.doi.org/10.1109/IEEESTD.1988.79638.

[42] X. Li, T. Stritch, K. Manley, M. Lucas, Limits and opportunities for miniaturizing ultrasonic surgical devices based on a Langevin transducer, IEEE Trans. Ultrason. Ferroelectr. Freq. Control 68 (7) (2021) 2543–2553, http://dx.doi.org/10.1109/TUFFC.2021.3065207.

[43] P. Gardonio, M.J. Brennan, On the origins and development of mobility and impedance methods in structural dynamics, J. Sound Vibr. 249 (3) (2002) 557–573, http://dx.doi.org/10.1006/jsvi.2001.3879.

[44] M. Schmid, E. Benes, W. Burger, V. Kravchenko, Motional capacitance of layered piezoelectric thickness-mode resonators, IEEE Trans. Ultrason. Ferroelectr. Freq. Control 38 (3) (1991) 199–206, http://dx.doi.org/10.1109/58.79604.

[45] D. Rizos, G. Feltrin, M. Motavalli, Structural identification of a prototype pre-stressable leaf-spring based adaptive tuned mass damper: Nonlinear characterization and classification, Mech. Syst. Signal Process. 25 (1) (2011) 205–221, http://dx.doi.org/10.1016/j.ymssp.2010.07.001.

[46] A. Lei, R. Xu, L.M. Borregaard, M. Guizzetti, O. Hansen, E.V. Thomsen, Impedance based characterization of a high-coupled screen printed PZT thick film unimorph energy harvester, J. Microelectromech. Syst. 23 (4) (2014) 842–854, http://dx.doi.org/10.1109/JMEMS.2013.2295625.

[47] R. Cleary, X. Li, M. Lucas, Incorporating direct metal laser sintered complex shaped Ti-6Al-4V components in ultrasonic surgical devices, J. Acoust. Soc. Am. 150 (3) (2021) 2163–2173, http://dx.doi.org/10.1121/10.0006379.

[48] M. Takasaki, Y. Maruyama, T. Mizuno, Resonance frequency tracing system for Langevin type ultrasonic transducers, in: 2007 International Conference on Mechatronics and Automation, IEEE, 2007, pp. 3817–3822, http://dx.doi.org/10.1109/ICMA.2007.4304183.

[49] A. Mathieson, A. Cardoni, N. Cerisola, M. Lucas, Understanding nonlinear vibration behaviours in high-power ultrasonic surgical devices, Proc. R. Soc. A 471 (2176) (2015) 20140906, http://dx.doi.org/10.1098/rspa.2014.0906.

[50] N. Wongdamnern, N. Triamnak, A. Ngamjarurojana, Y. Laosiritaworn, S. Ananta, R. Yimnirun, Comparative studies of dynamic hysteresis responses in hard and soft PZT ceramics, Ceram. Int. 34 (4) (2008) 731–734, http://dx.doi.org/10.1016/j.ceramint.2007.09.048.